Available online at www.sciencedirect.com
SCIENCE DIRECT®
Journal of Solid State Chemistry 178 (2005) 2008–2014
JOURNAL OF SOLID STATE CHEMISTRY
www.elsevier.com/locate/jssc

Why pressure induces an abrupt structural rearrangement in $PdTe_2$ but not in $PtTe_2$

C. Soulard[a], P.E. Petit[a], P. Deniard[a], M. Evain[a], S. Jobic[a,*], M.-H. Whangbo[b], A.-C. Dhaussy[c,1]

[a]*Laboratoire de Chimie des Solides (UMR 6502), Institut des Matériaux Jean Rouxel, 2 rue de la Houssinière, BP 32229, 44322 Nantes cedex 3, France*
[b]*Department of Chemistry, North Carolina State University, Raleigh, North Carolina 27695-8204, USA*
[c]*ESRF, 6 rue Jules Horowitz, BP 220, 38043 Grenoble Cedex, France*

Received 28 January 2005; received in revised form 29 March 2005; accepted 7 April 2005
Available online 4 May 2005

Abstract

High-pressure X-ray diffraction measurements were carried out for polymeric CdI_2-type compounds MTe_2 (M = Pt, Pd) to investigate if they undergo a structural phase transition under pressure as does $IrTe_2$. Up to 27 GPa at room temperature $PtTe_2$ does not undergo any structural phase transition. In contrast, however, an abrupt change in the inter-atomic distances occurs in $PdTe_2$ above 15.7 GPa at room temperature, and above 5 GPa at 300 °C, but the volume vs. pressure curve exhibits no discontinuity. To account for the differences between the isostructural compounds $PtTe_2$, $PdTe_2$ and $IrTe_2$, their electronic structures and bonding were analyzed on the basis of first principles electronic band structure calculations.

Keywords: $PdTe_2$; $PtTe_2$; X-ray diffraction

1. Introduction

The CdI_2-type transition metal dichalcogenides MQ_2 (M = transition metal, Q = chalcogen) consist of MQ_2 layers made up of edge-sharing MQ_6 octahedra, where adjacent MQ_2 layers are held together by van der Waals interactions. $IrTe_2$ adopts the polymeric CdI_2-type structure, i.e., a derivative of the CdI_2-type structure [1,2], in which adjacent MQ_2 layers have short $Q\ldots Q$ contacts thereby leading to a low c/a ratio, i.e., 1.38 instead of 1.67 expected on the basis of a classical hexagonal close stacking of the anions. From the viewpoint of the ionic electron counting leading to the charge balance $M^{4+}(Q^{2-})_2$, the occurrence of short interlayer $Q\ldots Q$ contacts is explained by considering the electron transfer from the p-block bands of Q to the d-block bands of M [3]. When the polymeric CdI_2-type $IrTe_2$ [2] (hereafter named h-$IrTe_2$) is subjected to pressure up to 32 GPa, it undergoes two structural phase transitions [4-6]. The hexagonal phase h-$IrTe_2$ is converted to a monoclinic-type structure (m-$IrTe_2$) at 5 GPa and at room temperature, and then to a pyrite structure (c-$IrTe_2$) at 32 GPa under laser heating.

$PtTe_2$ and $PdTe_2$ are similar to $IrTe_2$ in several structural and electronic properties under ambient conditions. They both adopt the polymeric CdI_2-type structure [7,8] with a low c/a ratio (i.e., 1.30 in $PtTe_2$ and 1.27 in $PdTe_2$). The three compounds $IrTe_2$, $PtTe_2$ and $PdTe_2$ have similar cell volumes per formula unit (i.e., 72.23(1) Å^3 for $IrTe_2$, 72.43(6) Å^3 for $PdTe_2$ and 73.35(4) Å^3 for $PtTe_2$), and their short Te…Te contacts are in the range of 3.44–3.56 Å. In addition, $IrTe_2$, $PtTe_2$ and $PdTe_2$ should be similar in electronic structure because the electronegativities of Ir, Pt and Pd are

*Corresponding author. Tel.: +33 2 40 37 39 22; fax: +33 2 40 37 39 95.
E-mail address: stephane.jobic@cnrs-imn.fr (S. Jobic).
[1]*Present address*: Laboratoire CRISMAT, UMR 6508, 6 boulevard Maréchal Juin, 14050 CAEN Cedex.

0022-4596/$ - see front matter © 2005 Elsevier Inc. All rights reserved.
doi:10.1016/j.jssc.2005.04.008

nearly the same (i.e., 2.20 for Ir and Pd, and 2.28 for Pt in Pauling scale), although MTe_2 (M = Pt, Pd) has one more valence electron per formula unit than does $IrTe_2$. Thus, one might suggest that the high-pressure behavior of MTe_2 (M = Pt, Pd) would be similar to that of $IrTe_2$. To test this speculation, we performed high-pressure X-ray diffraction experiments for MTe_2 (M = Pt, Pd) in both angle- and energy-dispersive configurations. MTe_2 (M = Pt, Pd) was not found to undergo a first-order structural phase transition up to 27 GPa. Only a sudden change in the pressure dependence of the interatomic distances was observed in $PdTe_2$ at about 19 and 6 GPa at room temperature and at 300 °C, respectively. To understand why $IrTe_2$, $PdTe_2$ and $PtTe_2$ behave differently under pressure, we compared their electronic structures on the basis of first principles electronic band structure calculations.

2. Synthesis and structure determination under pressure

2.1. Synthesis

A stoichiometric mixture of elemental powders (Pd sponge, 99.9% Aldrich; Pt powder, 325 mesh, 99.9 + %, Alfa Aesar; Te granules, 30 mesh, 99.99%, Aldrich) was ground and loaded into a quartz tube (~9 cm in length, 10 mm in diameter). The tubes were evacuated to 10^{-2} Torr, sealed and placed into a furnace whose temperature was raised to 850 °C at the rate of 5 °C per hour and kept there for 360 h, following the procedure of Lieth et al. [9] The powder sample was subsequently cooled to room temperature at the rate of 5 °C/h. X-ray powder diffraction data were collected on an INEL CPS 120 diffractometer (Debye–Scherrer geometry). The structure refinements were carried out using the JANA2000 software package [10]. The cell parameters obtained in the present work are in good agreement with those reported in the literature [7] (in italics and within parenthesis), i.e., $a = 4.027(1)$ (*4.026*) Å and $c = 5.223(2)$ (*5.221*) Å for $PtTe_2$, and $a = 4.037(2)$ (*4.037*) Å and $c = 5.132(2)$ (*5.126*) Å for $PdTe_2$. The corresponding volumes are 73.35(4) (*73.28*) $Å^3$ for $PtTe_2$ and 72.43(6) (*72.33*) $Å^3$ for $PdTe_2$.

2.2. Structure determination

Preliminary high-pressure energy-dispersive X-ray diffraction (EDX) measurements at 20 and 300 °C were carried out at the LURE (France). Experiments reported herein were performed in an angle-dispersive (ADX) mode on the ID30 beamline (ESRF, France) at room temperature (RT) for $PtTe_2$, and at RT and at 300 °C for $PdTe_2$. The experimental procedure has already been described elsewhere [11]. MTe_2 powder samples were ground to a fine powder in an agate mortar and loaded in the pressure chamber of a membrane-type diamond anvil cell (DAC). The pressure-transmitting medium added to provide quasi-hydrostatic pressure conditions was N_2 for the experiments at RT, and LiF for those at 300 °C. The ruby fluorescence method [12] was used to measure the in situ pressure.

The diffraction patterns were recorded up to 27 GPa for 2θ angles ranging from 2° to 20° (Figs. 1 and 2). For the 300 °C experiments, the $PdTe_2$ powder placed in the DAC was resistively heated. The storage ring was operated at 6 GeV and 7–15 mA (single-bunch mode). A channel-cut monochromator was used to select the wavelength of 0.3738 Å. The energy calibration was carried out using the K-edge of an iodine foil. The beam was focused via two multilayer mirrors settled in the Kirkpatrick-Baetz (KB) configuration, and then collimated with slits, thus defining a spot of 20 μm in

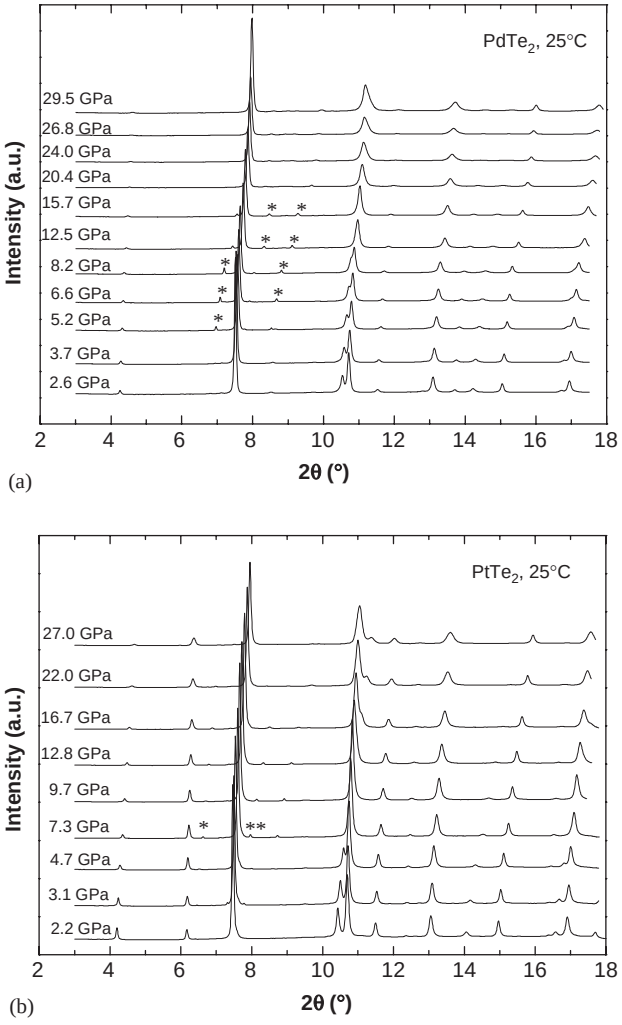

Fig. 1. Angle dispersive diffraction patterns of (a) $PdTe_2$ and (b) $PtTe_2$ under pressure during the decompression cycle at room temperature. The asterisks refer to the β-N_2 high-pressure phase.

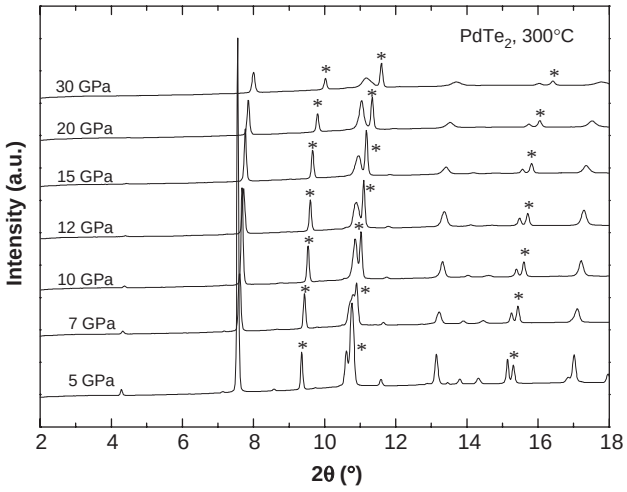

Fig. 2. Angle dispersive diffraction pattern of $PdTe_2$ up to 30 GPa at 300 °C during the compression cycle. The asterisks refer to the LiF phase.

diameter on the sample. An image plate located at 504.8 mm was employed to collect the pattern (exposure time of 90 s). The image was then converted into an $I(\theta)$ diffraction pattern using the fit2D software [13]. The lattice parameters and atomic positions were refined using the JANA2000 software package [10]. Each recorded diffraction patterns was refined using the Rietveld method with the conventional $P\bar{3}m1$ space group. The peak shape was modeled by a Thompson Cox Hasting function. The peak cutoff was set to $8 \times$ FWHM and the background was manually adjusted for simplicity because of peak overlapping in the whole range of diffraction pattern.

For each value of the external pressure at RT and 300 °C, it was possible to assign all the diffraction peaks to the CdI_2-type structure. Extra peaks are observed due to the pressure-transmitting medium. At room temperature, these peaks appear above ~5 GPa and originate from the formation of the high-pressure phase of nitrogen, β-N_2 [14]. At 300 °C, the extra peaks correspond to a crystallized form of the pressure medium LiF. Rietveld refinements data (i.e., the cell parameters, the volumes and the z-coordinates of Te) at RT during the compression cycle are reported in Table 1 for $PdTe_2$, and Table 2 for $PtTe_2$. The refinement results of $PdTe_2$ at 300 °C are given in Table 3. The crystal structures of $IrTe_2$, $PdTe_2$ and $PtTe_2$ at 0.1 MPa and 27 GPa are compared in Table 4.

2.3. Pressure-induced structural change

The pressure dependence of the M–Te, the intralayer Te–Te and the interlayer Te–Te distances at RT is summarized in Fig. 3 for $PtTe_2$, and in Fig. 4 for $PdTe_2$. As a function of pressure, the Pt–Te and the Te–Te distances of $PtTe_2$ exhibit a gradual change, and their distances keep the same trend (Fig. 3), i.e., intralayer Te–Te > interlayer Te–Te > Pt–Te. However, the corresponding distances of $PdTe_2$ undergo an abrupt change at ~19 GPa (Fig. 4). Namely, below ~19 GPa,

Table 1
Pressure dependence of the cell parameters, the cell volume V and the z coordinate of Te of $PdTe_2$ at room temperature during the compression cycle

Pressure (GPa)	Cell parameters			z
	a	c	V	
2.6	4.006(1)	5.032(1)	69.93(3)	0.275(2)
3.7	3.995(2)	5.004(2)	69.16(3)	0.277(2)
5.2	3.976(1)	4.963(1)	67.97(2)	0.275(2)
6.6	3.962(1)	4.932(1)	67.05(2)	0.277(2)
8.2	3.947(1)	4.899(1)	66.09(3)	0.280(2)
12.5	3.910(1)	4.822(2)	63.85(3)	0.289(3)
15.7	3.898(4)	4.752(3)	62.52(4)	0.296(3)
20.4	3.851(1)	4.764(1)	61.19(3)	0.343(3)
24.0	3.830(2)	4.748(3)	60.32(5)	0.341(3)
26.8	3.812(3)	4.736(3)	59.61(6)	0.339(3)
29.5	3.794(4)	4.722(4)	58.88(9)	0.337(5)

Table 2
Pressure dependence of the cell parameters, the cell volume V and the z coordinate of Te of $PtTe_2$ at room temperature during the compression cycle

Pressure (GPa)	Cell parameters			z
	a	c	V	
2.2	4.009(1)	5.100(2)	70.98(2)	0.282(4)
3.1	4.001(1)	5.054(1)	70.06(1)	0.276(3)
4.7	3.990(1)	4.995(2)	68.87(2)	0.280(4)
7.3	3.971(1)	4.907(2)	66.99(2)	0.290(4)
9.7	3.961(1)	4.829(2)	65.62(2)	0.308(4)
12.8	3.940(1)	4.767(2)	64.08(1)	0.286(4)
16.7	3.918(1)	4.687(2)	62.32(2)	0.281(5)
22	3.899(1)	4.597(3)	60.52(3)	0.278(7)
27	3.893(1)	4.536(4)	59.55(7)	0.273(9)

Table 3
Pressure dependence of the cell parameters, the cell volume V and the z coordinate of Te of $PdTe_2$ at 300 °C during the compression cycle

Pressure (GPa)	Cell parameters			z
	a	c	V	
5	3.993(1)	4.987(3)	68.8(1)	0.283(10)
7	3.976(3)	4.953(9)	67.8(2)	0.364(14)
10	3.937(1)	4.863(1)	65.3(1)	0.351(5)
12	3.914(3)	4.838(5)	64.2(1)	0.353(13)
15	3.927(4)	4.714(11)	63.0(1)	0.346(13)
20	3.894(30)	4.812(17)	63.2(7)	0.339(17)
30	3.835(9)	4.781(7)	60.9(2)	0.333(9)

Table 4
Crystal structures of the polymeric CdI_2-type structures of $PdTe_2$, $PtTe_2$ and $IrTe_2$ at 0.1 MPa and 27 GPa at ambient temperature

	$IrTe_2$		$PdTe_2$		$PtTe_2$	
	0.1 MPa [a]	27 Gpa[b]	0.1 MPa [c]	27 GPa [d]	0.1 MPa [c]	27 GPa [d]
a (Å)	3.9284(2)	3.771	4.037(3)	3.812(3)	4.026(5)	3.893(1)
c (Å)	5.4040(1)	4.829	5.126(4)	4.736(3)	5.221(5)	4.536(4)
V (Å^3)	72.22(1)	59.12	72.33(9)	59.61(6)	73.28(9)	59.55(7)
c/a	1.38	1.28	1.27	1.24	1.3	1.17
Z	0.2536(1)	0.283	0.247(5)	0.339(3)	0.254(5)	0.273(9)

[a]Refs. [2,3c].
[b]The cell parameters were taken from experiment, and the z value of Te from geometry optimization.
[c]Ref. [9].
[d]This work.

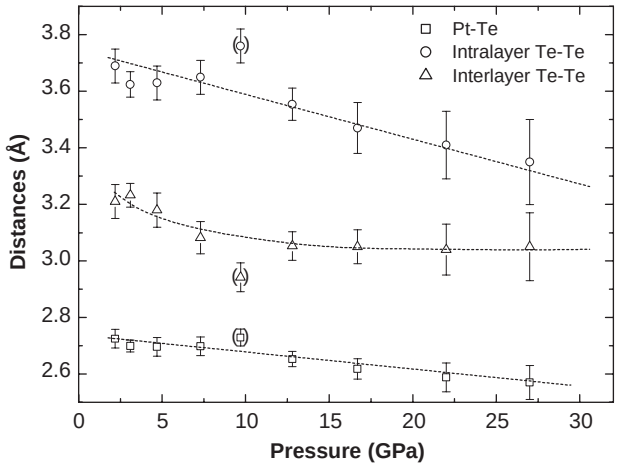

Fig. 3. Pressure dependence of the Pt–Te, the intralayer Te–Te and the interlayer Te–Te distances of $PtTe_2$ at room temperature. The brackets indicate that the data points collected at 9.2 GPa do not follow the smooth variation of the interatomic distances vs. pressure curve.

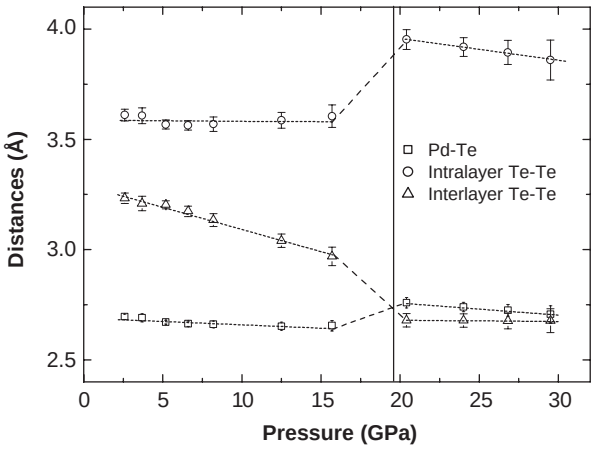

Fig. 4. Pressure dependence of the Pd–Te, the intralayer Te–Te and the interlayer Te–Te distances of $PdTe_2$ at room temperature. The vertical line represents a hypothetical frontier between the CdI_2-type structure (below ~19 GPa) and the modified CdI_2-type structure (above ~19 GPa).

the distances show the ordering, intralayer Te–Te > interlayer Te–Te > Pd–Te, as in the case of $PtTe_2$. Above ~19 GPa, they show the ordering, intralayer Te–Te > Pd–Te > interlayer Te–Te, so that the structure of $PdTe_2$ above ~19 GPa can be described as made up of $\frac{2}{\infty}$ [Te] double sheets encapsulating Pd atoms. The Te network of $PdTe_2$ above ~19 GPa exhibit similar structural features to the As-type high-pressure form of elemental Te [15] (Fig. 5). The short Te–Te distances of ~2.68 Å are even shorter than those found in elemental tellurium or in $[Te_n]^{2-}$ anions (i.e. ~2.75 Å) [16].

To gain some insight into the abrupt structural change of $PdTe_2$ at RT, additional experiments were performed at 300 °C up to 27 GPa (Fig. 2). The results of the refinements and the pressure dependence of the Pd–Te and Te–Te distances at 300 °C are summarized in Table 3 and Fig. 6. The pressure dependence of the Pd–Te and Te–Te distances at 300 °C is similar to that observed at RT. Only the pressure at which the abrupt distance change occurs is modified. The higher the temperature, the lower the pressure necessary for the structural reorganization (i.e., ~6 GPa at 300 °C vs. ~19 GPa at RT).

The abrupt structural change in $PdTe_2$ cannot be a first-order phase transition because the cell volume decreases smoothly with pressure as shown in Fig. 7. It is expected that the structure rearrangement is associated with a second-order phase transition, although this cannot be ascertained from our preliminary calculations based on the thermodynamic potentials derived from the first derivative of the volume. In summary, unlike the case of $IrTe_2$, both $PtTe_2$ and $PdTe_2$ do not undergo a first-order structural phase transition under the pressure and temperature ranges employed in our experiments. However, in contrast to the case of $PtTe_2$, $PdTe_2$ seems to display a second-order phase transition beyond a certain pressure, which decreases upon increasing the temperature. To account

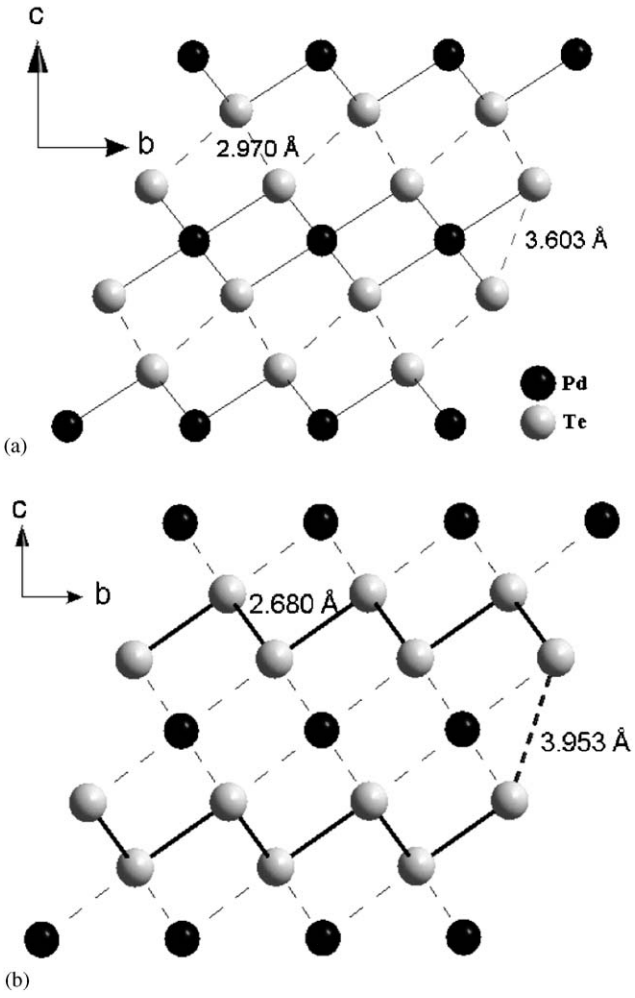

Fig. 5. Projection views of $PdTe_2$ at (a) 15 GPa and (b) 20 GPa.

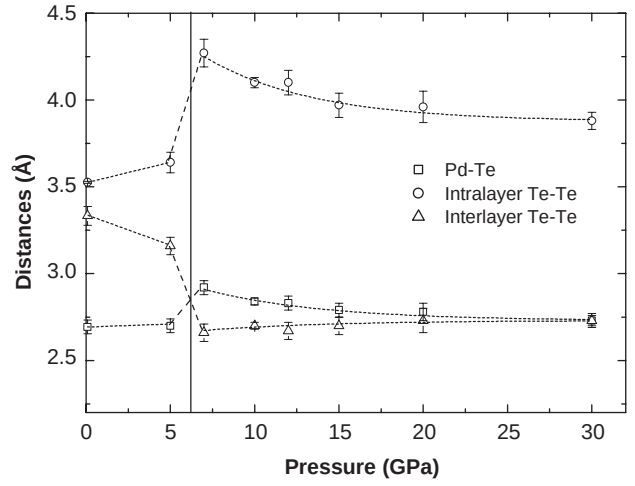

Fig. 6. Pressure dependence of the Pd–Te, the intralayer Te–Te and the interlayer Te–Te distances of $PdTe_2$ at 300 °C.

for this difference between MTe_2 (M = Pt, Pd) and $IrTe_2$, we compare their electronic structures in the next section.

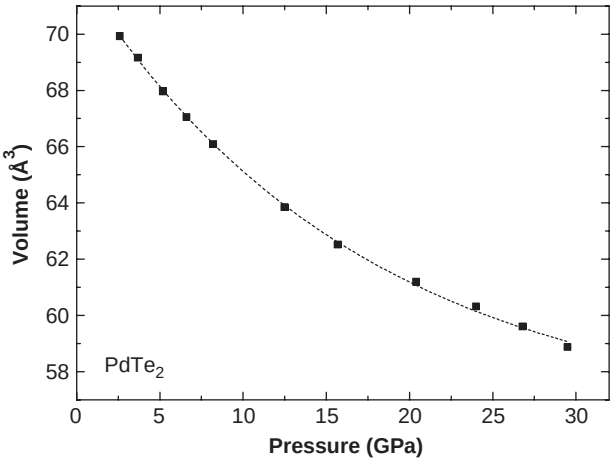

Fig. 7. Pressure dependence of the cell volume of $PdTe_2$. B_0 = 101.5 GPa and $V_0 = 71.29$ Å^3 are obtained from the Birch-Murnaghan second-order equation of state fit.

It is of interest to consider why such an abrupt structural change as observed for $PdTe_2$ does not occur in $PtTe_2$. We note from Fig. 4 that, when the pressure increased beyond ~19 GPa, the interlayer Te–Te distance collapses to form the $\frac{2}{\infty}$[Te] double sheets while increasing the Pd–Te bond length (from ~2.70 Å to ~2.80 Å). In other words, the strengthening of the Te–Te bonding takes place at the expense of weakening the Pd–Te bonding. The Pt 5*d* orbitals are more extended than the Pd 4*d* orbitals, so that the Pt–Te bond is more strongly covalent bonded than the Pd–Te bond. Therefore, it would be energetically unfavorable to decrease the interlayer Te–Te bonding at the expense of increasing the Pt–Te bonding.

3. Electronic structures of $IrTe_2$, $PdTe_2$ and $PtTe_2$

3.1. Computational details

First principles linearized full potential plane wave (FP-LAPW) calculations with non-spin-polarization were carried out for the CdI_2 structures of $IrTe_2$, $PtTe_2$ and $PdTe_2$ using the WIEN2k program package [17] within the generalized gradient approximation [18] for the exchange-correlation energy. The cell parameters and the atomic positions used for calculation were the experimental values taken from the literature (at 0.1 MPa), from our Rietveld refinements (at 27 GPa) for $PtTe_2$ and $PdTe_2$, and from our geometry optimization with the cell parameters taken from the high-pressure experiments for $IrTe_2$. For the 0.1 MPa structure, we employed the muffin-tin radii of 2.5 au for the metal and 2.4 au for Te. For the 27 GPa structure, we employed the muffin-tin radii of 2.4 au for both elements. The basis set cutoff parameters were

$G_{max} = 14\,\text{Bohr}^{-1}$ and $R_{mt}K_{max} = 8$. Integrations over the irreducible wedge of the Brillouin zone were performed using a 200k-point regular mesh (24k-points in the irreducible zone).

3.2. Density of states and oxidation states

The plots of the electronic DOS calculated for $IrTe_2$, $PtTe_2$ and $PdTe_2$ are compared in Fig. 8. The solid lines refer to the total DOS curves, the dotted lines and thick lines to the partial DOS for the *d* orbitals of the transition metal atoms and for the *p* orbitals of Te, respectively, and the vertical lines to the Fermi level. In capturing the essential features of the DOS curves, one often considers the oxidation state of the metal atoms. With the charge balance $(Ir^{3+})(Te^{1.5-})_2$ for h-$IrTe_2$, the oxidation state Ir^{3+} (d^6) given by the ionic electronic counting scheme predicts that the t_{2g} bands are completely filled and the e_g-block bands are empty. These predictions are only in approximate agreement with the total and partial DOS plots shown in Fig. 8a. The e_g-block bands of h-$IrTe_2$ may be assigned to the energy region between 1.4 and 3.6 eV. With the ionic picture [19–21] for a transition metal d^6 ion in an octahedral site, in which the main group ligand atoms are assumed to have the inert gas electron configuration (e.g., Te^{2-}), the t_{2g}-block bands are completely filled and the e_g-block bands are completely empty. Furthermore, in this picture, the metal orbitals should be the dominant character of the t_{2g}- and e_g-block bands. However, in the e_g-block bands of Fig. 8a, the Ir *d*-orbital contribution is smaller than the Te orbital contribution by a factor of two or greater. Thus, the "missing" Ir *d*-orbital contribution in the e_g-block bands occurs in the bands lying below them. Consequently, the actual amount of the occupied *d* electron density is greater than six.

In a similar manner, one may assign the e_g-bands of $PdTe_2$ and $PtTe_2$ to the energy region between −0.2 and 2.2 eV. If the oxidation state of +4 is assumed for the metal *M* of MTe_2 (*M* = Pt, Pd), the *d* electron count for *M* would be d^6 so that the e_g-block bands should be empty. However, the partial DOS plots of Figs. 8b and c reveal that the e_g-block bands are dominated by the Te *p*-orbital contributions. Therefore, the amount of occupied *d* electron density in MTe_2 (*M* = Pt, Pd) could be close to 10 as if the metal was in the oxidation state close to 0. As has been pointed out already [19–21], the concept of the ionic electron counting scheme becomes inadequate and leads to an erroneous picture for the electronic structures for compounds of late transition metal atoms with weak to medium electronegative main group elements such as Te.

4. Discussion and concluding remarks

It is noted that the shortest interlayer Te…Te distances of MTe_2 under ambient conditions (3.46 Å

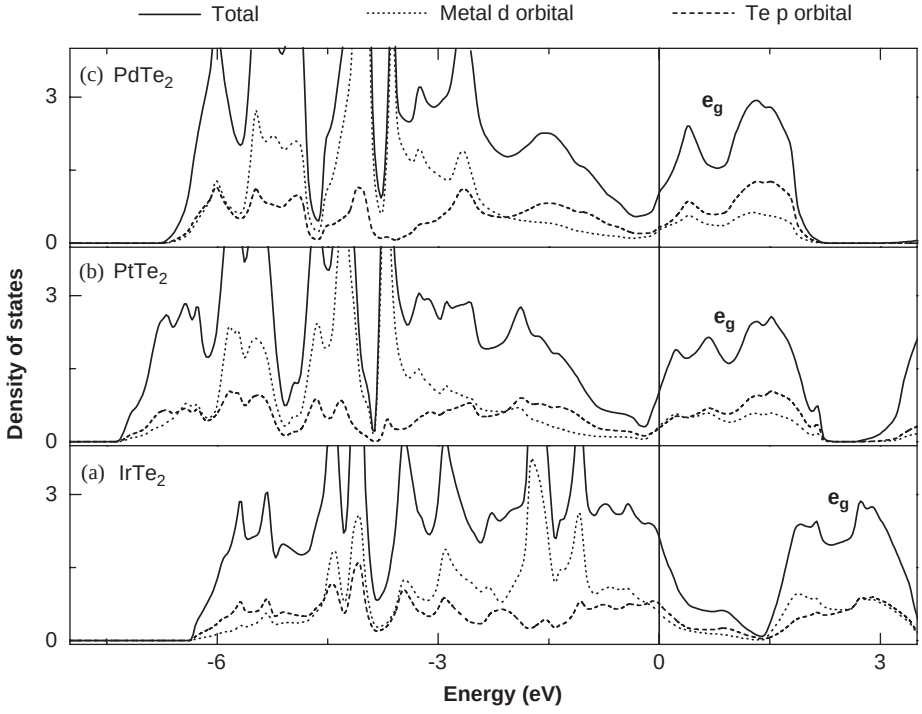

Fig. 8. Plots of the total DOS (solid line), the partial DOS for the metal *d* orbitals (dotted line) and the DOS for the Te *p* orbitals (dashed line): (a) $IrTe_2$, (b) $PtTe_2$ and (c) $PdTe_2$.

for M = Pt and 3.33 Å for M = Pd) are comparable to the shortest interchain Te…Te distance (3.47 Å) in trigonal tellurium [22] and the shortest interlayer Te…Te distance (3.47 Å) in monoclinic tellurium [23]. Furthermore, the hexagonal net of the As-type tellurium [15a] is quite similar in structure to that of MTe$_2$, and so are their interlayer Te…Te distances (3.48 Å). These observations suggest that the charge distribution on tellurium in MTe$_2$ is quite similar to that in elemental tellurium. Therefore, it is appealing to conclude that the tellurium of MTe$_2$ has the oxidation state close to 0 rather than to −2, and hence the metal M of MTe$_2$ (M = Pt, Pd) has the oxidation state close to 0. This conclusion is consistent with the observation that M and Te have a similar electronegativity (2.1 for Te and ~2.2 for M). To a first approximation, therefore, the M–Te bonds of MTe$_2$ (M = Pt, Pd) are primarily covalent in character. Consequently, it is difficult to describe the electronic structure of MTe$_2$ in terms of the ionic electron counting scheme.

The pressure induced structural transitions of IrTe$_2$ is explained by noting that an external pressure applied shortens mainly the Te…Te distances to raise the energy of the Te p-block bands, and this induces electron transfer from the Te p-block bands to the Ir d-block bands, because the d-block levels are not completely filled. As discussed in the previous section, the d-block energy levels of MTe$_2$ (M = Pt, Pd) are practically completely filled. Consequently, the electron transfer Te $p \rightarrow M$ d cannot take place even if the Te p-block bands are raised in energy by shortening the Te…Te distances. This explains why such pressure-induced structural phase transitions as observed in h-IrTe$_2$ do not take place in MTe$_2$ (M = Pt, Pd).

Nevertheless, MTe$_2$ (M = Pd, Pt) exhibits a slightly different response to pressure. When the pressure increased beyond ~19 GPa, the interlayer Te–Te distance of PdTe$_2$ collapses to form the $^2_\infty$[Te] double sheets while increasing the Pd–Te bond length. A similar structural change does not occur in PtTe$_2$, probably because the Pt–Te bond is more strongly covalent bonded than the Pd–Te bond.

Acknowledgments

The authors thank J.-P. Itié and P. Munsch (LURE), and M. Mezouar, T. Le Bihan, and W. Crichton (ESRF) for the technical support they provided during the high-pressure experiments. ESRF is acknowledged for providing beam time (project HS-1909). The work at NCSU was supported by the Office of Basic Energy Sciences, Division of Materials Sciences, US Department of Energy, under Grant DE-FG02-86ER45259.

References

[1] E.F. Hocking, J.G. White, J. Phys. Chem. 64 (1960) 1042.
[2] S. Jobic, P. Deniard, R. Brec, J. Rouxel, A. Jouanneaux, A.N. Fitch, Z. Anorg. Allg. Chem. 598/599 (1991) 1999.
[3] (a) S. Jobic, R. Brec, J. Rouxel, J. Alloys Compd. 178 (1992) 253; (b) E. Canadell, S. Jobic, R. Brec, J. Rouxel, M.-H. Whangbo, J. Solid State Chem. 99 (1992) 189; (c) S. Jobic, R. Brec, J. Rouxel, J. Solid State Chem. 96 (1992) 169.
[4] J.-M. Léger, A.S. Pereira, J. Haines, S. Jobic, R. Brec, J. Phys. Chem. Solid 61 (2000) 27.
[5] S. Jobic, R. Brec, C. Château, J. Haines, J.-M. Léger, H.-J. Koo, M.-H. Whangbo, Inorg. Chem. 39 (2000) 4370.
[6] S. Jobic, R. Brec, A. Pasturel, H.-J. Koo, M.-H. Whangbo, J. Solid State Chem. 162 (2001) 63.
[7] S. Furuseth, K. Selte, A. Kjekshus, Acta Chem. Scand. 19 (1965) 257.
[8] D. Dai, H.-J. Koo, M.-H. Whangbo, C. Soulard, X. Rocquefelte, S. Jobic, J. Solid State Chem. 173 (2003) 114.
[9] R.M.A. Lieth, C.J.M. Terhell, Preparation and crystal growth of materials with layered structures, D. Reidel Publishing Company, Dordrecht, Holland, 1977.
[10] V. Petricek, M. Dusek, JANA2000. Crystallographic computing system, Institute of Physics, Praha, Czech Republic, 2000.
[11] W. Paszkowicz, Nucl. Instrum. Methods B 198 (2002) 142.
[12] J. Xu, H.K. Mao, P.M. Bell, Science 232 (1986) 1404.
[13] A.P. Hammersley, S.O. Svensson, M. Hanfland, A.N. Fitch, D. Häusermann, High Press. Res. 14 (1996) 235.
[14] D. Schiferl, D.T. Cromer, R.R. Ryan, A.C. Larson, R. Le Sar, R.L. Mills, Acta Crystallogr. C. 39 (1983) 1151.
[15] (a) S.S. Kabalkina, L.F. Vereshchagin, B.M. Shulenin, J. Exptl. Theor. Phys. 45 (1963) 2073 [Soviet Phys. JETP 18 (1964) 1422]; (b) C. Soulard, X. Rocquefelte, M. Evain, S. Jobic, H.-J. Koo, M.-H. Whangbo, J. Solid State Chem. 177 (2004) 4724.
[16] (a) I. Schewe, P. Boettcher, Z. Naturforsch. 45 (1990) 417; (b) J. Getzschmann, P. Boettcher, W. Kaluza, Z. Kristallogr. 211 (1996) 90; (c) W.S. Sheldrick, B. Schaaf, Z. Naturforsch. 49 (1994) 993; (d) B. Eisenmann, H. Schaefer, Angew. Chem. 90 (1978) 731; (e) P. Boettcher, R. Keller, J. Less-Common Metals 109 (1985) 311; (f) D.Y. Valentine, O.B. Cavin, H.L. Yakel jr, Acta Crystallogr. B 33 (1977) 1389; (g) P. Boettcher, R. Keller, Z. Anorg. Allg. Chem. 542 (1986) 144; (h) E. Zintl, H. Kaiser, Z. Anorg. Allg. Chem. 211 (1933) 113.
[17] P. Blaha, K. Schwarz, G. Madsen, D. Kvasnicka, J. Luitz, WIEN2k, An Augmented Plane Wave + Local Orbitals Program for Calculating Crystal Properties (Karlheinz Schwarz, Techn. Universität Wien, Austria), 2001. ISBN:3950103112. See also: http://www.wien2k.at/
[18] J.P. Perdew, S. Burke, M. Ernzerhof, Phys. Rev. Lett. 77 (1996) 3865.
[19] J.A. Paradis, M.-H. Whangbo, R.V. Kasowski, New J. Chem. 17 (1993) 525.
[20] K.S. Lee, H.-J. Koo, D. Dai, J. Ren, M.-H. Whangbo, Inorg. Chem. 38 (1999) 340.
[21] K.S. Lee, H.-J. Koo, J. Ren, M.-H. Whangbo, J. Solid State Chem. 147 (1999) 11.
[22] C. Adenis, V. Langer, O. Lindqvist, Acta Crystallogr. C 45 (1989) 941.
[23] K. Aoki, O. Shimomura, S. Minomura, J. Phys. Soc. Japan 48 (1980) 551.